Available online at www.sciencedirect.com
SCIENCE DIRECT®
Journal of Nuclear Materials 350 (2006) 208–220
journal of nuclear materials
www.elsevier.com/locate/jnucmat

The development of a stress analysis code for nuclear graphite components in gas-cooled reactors

D.K.L. Tsang *, B.J. Marsden

Nuclear Graphite Research Group, School of Mechanical, Aerospace and Civil Engineering, The University of Manchester, P.O. Box 88, Manchester M60 1DQ, UK

Received 5 October 2005; accepted 30 January 2006

Abstract

Most of the UK nuclear power reactors are gas-cooled and graphite moderated. As well as acting as a moderator the graphite also acts as a structural component providing channels for the coolant gas and control rods. For this reason the structural integrity assessments of nuclear graphite components is an essential element of reactor design. In order to perform graphite component stress analysis, the definition of the constitutive equation relating stress and strain for irradiated graphite is required. Apart from the usual elastic and thermal strains, irradiated graphite components are subject to additional strains due to fast neutron irradiation and radiolytic oxidation. In this paper a material model for nuclear graphite is presented along with an example of a stress analysis of a nuclear graphite moderator brick subject to both fast neutron irradiation and radiolytic oxidation.

1. Introduction

Most of the UK operating nuclear reactors are graphite moderated and carbon dioxide cooled. For the reactor designer there are two main advantages for the use of gas as a coolant. Firstly the density of gas can be varied, allowing the design operating temperature to be chosen independently of the operating pressure. Thus a high gas temperature can be defined and an optimum pressure can then be selected separately, accounting for reactor safety and the economics of pumping power as well as pressure circuit costs. Secondly reactor operating conditions can be chosen such that the gas can undergo no phase change as a result of rising temperature or falling pressure, so gas cooling can be maintained even under fault conditions. Also gas flow and temperature can be simply and confidently predicted [1].

The early reactor designs [2] in the UK, e.g. Gleep, Bepo and Windscale piles, were graphite-moderated air-cooled reactors. Later, eight dual-purpose reactors (electric generation and plutonium production) were built at Calder Hall and Chapelcross which used carbon dioxide as a coolant. The simple well thought out design of these gas-cooled

* Corresponding author. Tel.: +44 1612754391.
E-mail address: Kwong-Lai.Tsang@manchester.ac.uk (D.K.L. Tsang).

0022-3115/$ - see front matter © 2006 Elsevier B.V. All rights reserved.
doi:10.1016/j.jnucmat.2006.01.015

graphite moderated reactors gave nearly 50 years of reliable operation. A rapid increase in electric power demand in the 1960s led to an increased program for power generation reactors. Nine Magnox stations were eventually built in the UK with a total net output of nearly 5000 MW(e).

The use of magnesium alloy fuel cladding and natural uranium metal fuel in Magnox reactors led to relatively low fuel ratings and outlet temperatures ≈360 °C, which meant that the plant tended to be large, and costly with relatively low efficiency. Therefore, a better and more advanced design was developed, the advanced gas-cooled reactor (AGR). The AGR design was based on a slightly enriched uranium dioxide fuel, encased in stainless steel cladding and arranged in clusters of small diameter pins. This fuel has the advantage that it is chemically inert in carbon dioxide up to very high temperatures. In addition the AGR operates at higher coolant pressure than the Magnox reactors giving a higher outlet temperature of ≈650 °C making the steam generation side more efficient.

The high temperature reactor (HTR) was the next step in the evolution of graphite moderated gas-cooled reactors. The change in coolant to helium opens up new possibilities in fuel design and higher operating temperatures. The HTR promises lower costs through higher core power, smaller plant size and replaceable moderator. The all ceramic fuel and helium coolant allow for a high outlet temperature of ≈1000 °C and lead to the possibility of using the heat directly for industrial processes. Interest was aroused around the world and led to the construction of experimental and prototypic reactors, e.g., DRAGON in the UK, Peach Bottom and Fort St. Vrain in the USA, and AVR and THTR in Germany. Interest in the HTR systems has continued to the present day in many countries for example the pebble bed modular reactor (PBMR) in South Africa, the high temperature engineering test reactor (HTTR) in Japan and the 10 MWt high temperature gas-cooled demonstration reactor (HTR-10) in China. The very high temperature reactor (VHTR) is now one of the most promising designs being considered by the international Generation IV initiative. One of the most exciting applications of the VHTR is the efficient production of hydrogen by the sulphur–iodine cycle.

In a gas-cooled reactor the properties of the graphite components are changed by fast neutron irradiation and, in the case of air or carbon dioxide-cooled reactors, by radiolytic oxidation. These irradiation induced changes can lead to the build up of significant stresses and deformation in the graphite components. Throughout reactor life it is essential that the graphite core structure remains sufficiently strong and undistorted in order to maintain fuel cooling, permit loading and unloading of the fuel and allow the necessary movements of control rods, in both normal and fault conditions.

In order to perform structural integrity assessments, the definition of the constitutive equation relating stress and strain in the irradiated graphite material is required. Apart from the elastic and thermal strain, graphite in nuclear reactors also experiences additional strains due to fast neutron irradiation. Irradiation creep and irradiation induced dimensional change are two most important of these irradiation strains. In some cases, irradiation creep strain is beneficial because of stress relief, especially in regions of high stress concentrations. Although the irradiation creep strain relaxes stresses generated by temperature gradients and the irradiation induced dimensional changes to some extent, significant component stresses can still be generated. Furthermore, the dimensional change strain in graphite components can lead to similar internal stress distributions to those generated by thermal loading and these additive stress distributions may be critical in design. Therefore, it is important to consider the effect of irradiation creep strain, thermal strains and dimensional changes in graphite component stress analysis.

Nuclear graphite component structural integrity assessments are usually carried out using the finite element method. In order to model the dimensional change, irradiation creep and material properties a complex material model is required. The models used are largely empirical and are based on material test reactor (MTR) irradiated graphite property data. The application of nuclear graphite constitutive equations using standard finite element techniques are further complicated as irradiation creep in graphite is considered not to conserve volume [3], i.e. with irradiation, the volume of graphite increases under tension loading and decreases under compression loading. Consequently, specially written coding is required to model the behaviour of irradiated graphite components.

A viscoelastic graphite model was first produced in the USA by Chang and Rashid [4]. Later, a model called VIENUS was created by JAERI in Japan for a HTTR graphite block by Iyoku et al.

[5]. In the UK, a model for two dimensions and axi-symmetric geometries was created using BERSAFE finite element code by Harper [6]. This was later developed using the ABAQUS [7] finite element programme by Whittaker [8] using a User MATerial (UMAT) subroutine to model Gilsocarbon graphite components in two dimensions.

A material model subroutine called MAN UMAT has been recently developed for nuclear graphite under fast neutron irradiation and radiolytic oxidation conditions. The subroutine can be used together with the ABAQUS finite element program to perform three-dimensional, time-integrated, non-linear irradiated graphite stress analyses. The subroutine has been used to study the graphite brick bore profile [9]. In this paper, the development of the MAN UMAT is presented.

2. Unirradiated nuclear graphite material properties

The mechanical properties of isotropic graphite are given in Table 1. The density of pure graphite crystals is 2.26 g/cm^3, however the density of the manufactured graphite has a much lower density as can be seen from Table 1. The lower density is due to gas evolution porosity and inter-crystalline cracks formed during the baking and graphitisation stages of graphite manufacture. The inter-crystalline cracking which gives graphite its unique unirradiated and irradiated properties is often referred to as Mrozowski cracks [10]. Mrozowski first proposed these cracks and suggested models for the edge linking of mutually oriented crystallites. He attributed the internal voidage to the basal plane micro-cracks produced during the anisotropic shrinkage of the crystallites on cooling from graphitising temperatures.

Table 1
Typical virgin material property for isotropic graphite

Material property of isotropic graphite	Values
Density	1.81 g/cm^3
Mean coefficient of thermal expansion (CTE)	4.35×10^{-6} (°C)$^{-1}$
Poisson's ratio	0.2
Dynamic Young's modulus	10 GPa
Ratio of SYM to DYM	0.84

In the UK nuclear industry, the coefficient of thermal expansion (CTE) is usually quoted in the range 20–120 °C although measurement over a larger range, say 20–400 °C yields more accurate value. The CTE is temperature dependent with an increase in temperature producing an increase in CTE. Poisson's ratio for elastic strain is assumed to be 0.2 and to be independent of irradiation.

The stress–strain curves for unirradiated isotropic graphite subjected to cyclic loading are shown in Fig. 1. When an external load is applied, the initial macro-deformation is governed by elastic shear and plastic deformation of individual crystallites, the latter causing a non-linear macro stress/strain response. A large permanent set occurs when the load is removed.

Most of the Young's modulus data are obtained by an ultrasound method. The method represents the slope of the stress–strain curve at the origin to represent the modulus and the modulus is referred to as the dynamic Young's modulus (DYM) E_d.

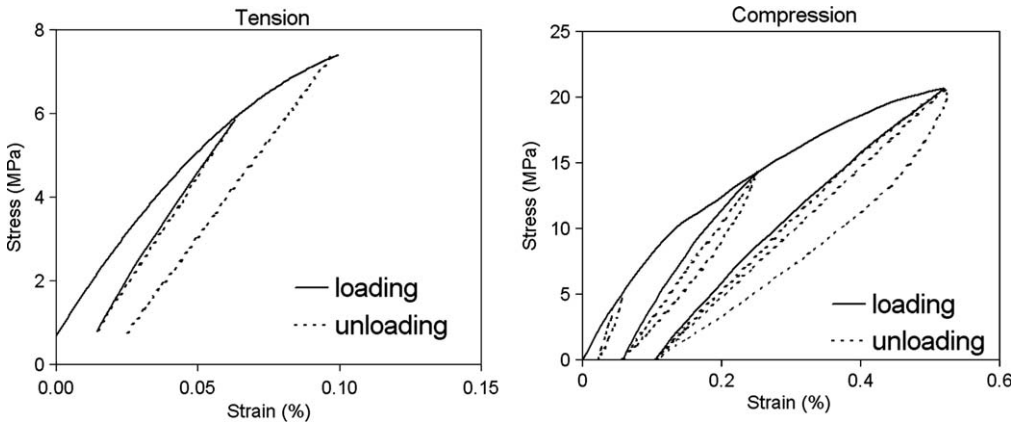

Fig. 1. Stress–strain curves for unirradiated graphite subjected to cyclic loading.

The Young's modulus can also be obtained in 'static' tests using strain gauges. This value is obtained from the average slope of an unload–load cycle of the stress–strain curve to define the recoverable elastic strain and is referred to as the static Young's modulus (SYM) E_s. In the UK nuclear industry the stress load level has been traditionally set to be less than or equal to half the tensile strength and hence does not include the permanent set strain observed in general static tests. The mean ratio of SYM to DYM is about $E_s/E_d = 0.84$ for unirradiated graphite depending on the load range over which it is measured. More information about relation between SYM and DYM of nuclear graphite has been published by Oku and Eto [11].

3. UK methodology for isotropic graphite irradiated in CO_2

There are two processes in nuclear reactors which modify the graphite properties significantly. The first process is the creation of lattice defects by the energetic radiation, principally the neutrons. The neutrons emitted in the fission process in the fuel of a thermal reactor lose their excess energy in collisions with the nuclei of the moderator atoms. A primary atomic displacement produced by a neutron–nuclei collision with a carbon atom produces a cascade of further displacements. Detailed calculations have been performed by a number of authors [12,13]. The calculations indicate that 200–1000 atoms are displaced by the most energetic collisions, spread out over a large volume, such that it is a good approximation to consider that the displacements occur at random. During irradiation, crystal interstitials and vacancies are formed when fast neutrons displace carbon atoms from their lattice positions. These point defects can recombine to form a vacancy or interstitial loop. The rate and extent to which the recombination takes place is dependent on the irradiation temperature. Measurements of the crystal lattice parameters using X-rays showed that the interlayer spacing increases while the atomic spacing in the layer decreases under irradiation. Direct transmission electron microscopy by Reynolds and Thrower [14] showed that the crystal growth is due to the formation and growth of interstitial dislocation loops. The large basal plane contractions can be explained by the collapse of linear vacancy groups, the two-dimensional analogue of the vacancy loop. In short, neutrons bombardment of graphite initially creates point defects, which, depending on the irradiation temperature lead to more complex defects with increasing irradiation fluence. The lattice defects lead to the changes in the properties of the graphite.

The second process is radiolytic oxidation. Under fault conditions graphite oxidation by thermal reaction can predominate in the high temperature gas-cooled reactor. However, thermal oxidation is insignificant in the lower temperature CO_2-cooled graphite moderators. Radiolytic oxidation occurs when CO_2 is decomposed by ionising radiation to give reactive oxidising species. The rate of graphite oxidation is proportional to the rate of production of the oxidising species, which is itself a function of radiation intensity and gas pressure (but is substantially independent of temperature). Reviews which summarise the relevant information on oxidation of graphite due to radiolytic activation of carbon dioxide and the combination of the effects of oxidation with those of irradiation damage to predict the operational life of the graphite moderator can be found in Best et al. [15] and Kelly [16].

In this section changes in the structural, mechanical and thermal properties of isotropic graphite due to fast neutron irradiation and radiolytic oxidation are given. Property variations are given as a function of fast neutron fluence, temperature, fractional weight loss and graphite oxidation rate. These field variables are calculated using other analysis programs. The units for irradiation fluence and irradiation temperature are expressed in terms of equivalent DIDO nickel dose (EDND) and °C.

3.1. Young's modulus

Following irradiation the stress–strain relationship become more linear and the permanent set is decreased. Experiments to determine the elastic response of irradiated graphite have tended to concentrate on the dynamic Young's modulus as the basic of measurement. At low irradiation fluence levels there is a rapid increase in modulus followed by a constant state. At higher fluence levels the Young's modulus shows a gradual increase to a peak followed by a fall (see Fig. 2).

There are two distinct mechanisms involved in these changes, firstly due to changes in the elastic constants of the graphite crystals and secondly due to changes in the bulk structure of the graphite. The first of these which is responsible for the initial rise in Young's modulus, is attributed to the pinning of the crystal basal planes and this effect soon

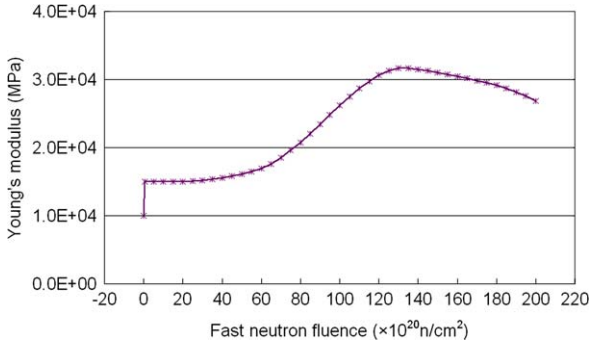

Fig. 2. Young's modulus of an irradiated isotropic graphite at temperature 550 °C.

saturates. The second, is attributed to differential straining of the polycrystalline micro-structure due to crystal growth and porosity closure leading to an increase in modulus. However, at even large crystal strains micro-cracks are generated which eventually leads to the reduction of the modulus and loss of strength.

The irradiated DYM E_d can be described by the following equation:

$$\frac{E_d}{E_0} = P(T) \times S(\gamma, T) \times W(x), \tag{1}$$

where E_0 is the unirradiated DYM, P is the saturated pinning term to account for the pinning of mobile dislocations and is assumed to be a function of temperature only, S is the structure term to allow for structural changes due to irradiation damage and is a function of fluence γ and irradiation temperature T, and W is the weight loss term. The weight loss term is given as a function of fractional weight loss by [16]:

$$W(x) = \exp(-\lambda_1 x), \tag{2}$$

where x is the fractional weight loss and $\lambda_1 = 3.4$ is an empirical constant. The irradiated SYM is given by

$$\frac{E_s}{E_0} = f_i \times P(T) \times S(\gamma, T) \times W(x), \tag{3}$$

where f_i is a mean ratio of the irradiated SYM to DYM.

The pinning term is assumed to saturate instantaneously at low fluence. It is also assumed that the pinning term and the structure term can be calculated separately and combined using the multiplication law given in Eq. (1) above. These assumptions are required as it is considered that the pinning term does not affect irradiation creep but the structural changes do. It is assumed that Poisson's ratio is not a function of temperature, fluence or weight loss, and stays constant at a value of 0.2.

3.2. Irradiation creep

The fact that graphite undergoes irradiation-induced creep is important because, as graphite moderator blocks in a nuclear reactor are subjected to significant temperature and irradiation fluence gradients, and irradiation induced dimensional changes in graphite are both temperature and fluence dependent, these lead to self-induced stresses to be imposed on the blocks. These stresses would build up to levels exceeding the fracture strength of graphite [17] in many cases if these stresses were not relieved by irradiation creep [18].

The creep coefficient is considered to be equal in tension and compression for a given graphite. Irradiation creep strain is defined as 'the difference in dimensions between a stressed sample and a sample with the same properties as the stressed sample irradiated unstressed' [19]. It has been postulated that the irradiation creep in graphite is due to slip in the basal plane activated by the neutron irradiation and not by internal stress. The creep rate is considered to be proportional to stress and practically independent of temperature in the range 300–650 °C.

Irradiation creep can be characterised by a transient stage followed by a linear stage. The magnitude of both primary transient creep and secondary creep was found to be proportional to stress and inversely proportional to the unirradiated modulus of elasticity [20].

3.3. Coefficient of thermal expansion

Fast neutron irradiation fluence modifies the coefficient of linear thermal expansion (CTE). This change is a function of the irradiation fluence, irradiation temperature and actual temperature. However, graphite CTE does not appear to be affected by radiolytic oxidation [16]. The CTE is used to evaluate thermal strain and consequently the calculation of its value involves a change in temperature or in CTE. The instantaneous coefficient of linear thermal expansion α_i at temperature T can be written as

$$\alpha_i(T) = \frac{d\varepsilon^{th}}{dT}, \tag{4}$$

where the subscript i represents instantaneous value. Therefore the thermal strain can be written as

$$\varepsilon^{\text{th}}(T) = \int_{T_{\text{ref}}}^{T} \alpha_{\text{i}}(\theta)\,\mathrm{d}\theta, \tag{5}$$

where θ is a dummy variable of integration and T_{ref} (°C) is a reference temperature. As the CTE of graphite is temperature dependent, most practical applications require the mean CTE over a temperature range. For convenience it is useful to introduce the reference temperature $T_{\text{ref}} = 20$ °C and refer to the mean CTE over a temperature range:

$$\bar{\alpha}_{(T_{\text{ref}}-T)} = \frac{1}{(T_{\text{ref}} - T)} \int_{T_{\text{ref}}}^{T} \alpha_{\text{i}}(\theta)\,\mathrm{d}\theta, \tag{6}$$

where $\bar{\alpha}_{(T_{\text{ref}}-T)}$ is the mean CTE over the temperature range T_{ref}–T °C for either unirradiated or irradiated graphite. The mean CTE over any desired temperature range T_1–T_2 °C can then be expressed as

$$\bar{\alpha}_{(T_1-T_2)} = \frac{1}{(T_2 - T_1)}\left[(T_2 - T_{\text{ref}})\bar{\alpha}_{(T_{\text{ref}}-T_2)} - (T_1 - T_{\text{ref}})\bar{\alpha}_{(T_{\text{ref}}-T_1)}\right]. \tag{7}$$

Using Eq. (6), the thermal strain caused by the temperature difference from T_{ref} to T can be rewritten as

$$\varepsilon^{\text{th}} = \bar{\alpha}_{(T_{\text{ref}}-T)}(T - T_{\text{ref}}). \tag{8}$$

As is the case for unirradiated CTE, irradiated CTE is usually quoted over the temperature range 20–120 °C in the UK. However, the irradiated mean CTE over some other temperature range 20–T °C can be written as [21]:

$$\bar{\alpha}_{(20-T)} = \bar{\alpha}_{(20-120)} + \overline{B}, \tag{9}$$

where $\overline{B}$ is a function of the actual temperature T and the irradiated mean CTE $\bar{\alpha}_{(20-120)}$ is a function of irradiation fluence and temperature. The experimentally determined irradiated mean CTE can be obtained from measurement made on graphite samples irradiated in a MTR.

Early irradiation creep experiments [22] have shown that changes to the thermal expansion coefficient in irradiated specimens appear to be dependent on the magnitude of creep strain. Those specimens with a significant amount of compressive creep strain have a higher CTE, measured in the direction of stress, compared with the unstressed specimens, whereas specimens with significant tensile creep strain have a lower thermal expansion coefficient compared to the unstressed specimens.

3.4. Dimensional change

Radiation damage by fast neutron fluence causes crystal growth in the *c*-axis direction and shrinkage in the *a*-axis direction [23]. The effect of these irradiation induced crystal changes on the dimensional changes in isotropic moderator graphites has been reviewed by Neighbour [24]. Neutron irradiation of polygranular reactor graphites results in initial bulk shrinkage at low neutron fluence, leading eventually to a net expansion of the graphite with increasing fluence. Above irradiation temperatures of 300 °C, the initial effect of neutron irradiation on the microstructure of the graphite is closure of small pores and cracks as a result of *c*-axis expansion and contraction of the crystallites in the *a*-axis causing the initial bulk shrinkage of the graphite. The reversal of shrinkage, called 'turnaround', is believed to begin when the shrinkage cracks are unable to accommodate new irradiation-induced crystallite growth. At higher irradiation temperatures, turnaround occurs at lower neutron fluence. This is attributed to a reduction in the extent of accommodation available for irradiation-induced *c*-axis expansion as a result of closure of Mrozowski cracks by thermal expansion. With further crystallite growth after turnaround, internal stresses develop to the point where new micro-cracks and pores begin to appear.

The amount of dimensional change is assumed to be a function of irradiation fluence and irradiation temperature. However, there are little experimental data [25] for the combined effect of the irradiation and radiolytic oxidation in a CO_2 atmosphere. To enable structural integrity calculations to be carried out it has been assumed that for a given temperature, the dimensional change against fluence can be represented by the linear combination of two curves [16]:

- Curve A: maximum effect of the weight loss. The curve continues to shrink over the full fluence range. Curve A is obtained from theoretical consideration of the relationship between crystal and polycrystalline dimensional change rates and CTE [13], and data obtained on graphite crystal structures [23].
- Curve B: no weight loss. Curve B is an empirical curve obtained from graphite irradiation experiments. At low fluence Curve B follows Curve A, but gradually the rate of shrinkage decreases, eventually passing through a maximum shrinkage value before reversing, often referred to as 'turnaround'.

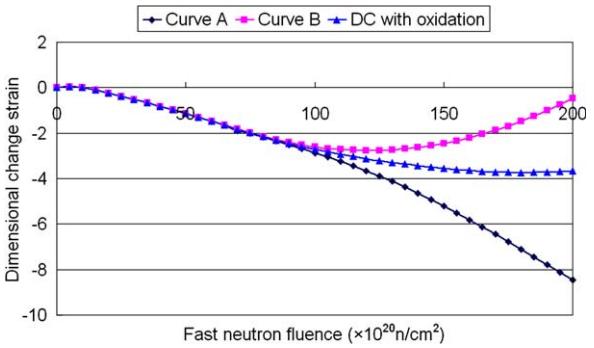

Fig. 3. Schematic of a dimensional change with radiolytic oxidation.

For a given fluence and temperature, the dimensional change strain can be determined by linear interpolation between the positions on Curve A and Curve B (see Fig. 3):

$$\varepsilon^{dc} = \phi \times \varepsilon^{dc}_{A} + (1-\phi) \times \varepsilon^{dc}_{B}, \tag{10}$$

where ε^{dc} is the dimensional change strain, ε^{dc}_{A} is the dimensional change strain for Curve A as a function of fluence and temperature, ε^{dc}_{B} is the dimensional change strain for Curve B as a function of fluence and temperature, ϕ is the fractional distance between Curve B and Curve A, which is a function of the graphite oxidation rate.

It should be noted that this is an approximation for the effect of radiolytic oxidation on the dimensional changes of graphite due to irradiation, permitting interpolation between two curves, Curve B corresponding to zero oxidation rate and Curve A to oxidation rate sufficiently fast that micro-crack closure due to neutron irradiation is prevented. However, the actual situation is probably more complex and requires further study.

It has been postulated that similar to CTE, the irradiation creep perturbs the graphite microstructure enough to produce significant modifications to the dimensional change rate (see [19,26]). A correction term in the dimensional change has been proposed by Kelly and Burchell [19].

4. Constitutive equations

The complex material behaviour of irradiated graphite has been implemented into the ABAQUS [5] finite element code using a User MATerial subroutine (UMAT). At the beginning of each increment, ABAQUS estimates the total strain within the model. There are two functions performed by the UMAT subroutine. Firstly, it updates the stresses to their values at the end of the increment from the estimated total strain. Secondly, it provides the graphite material Jacobian matrix $\partial\Delta\boldsymbol{\sigma}/\partial\Delta\boldsymbol{\varepsilon}^{e}$ for the mechanical constitutive model, where $\Delta\boldsymbol{\sigma}$ and $\Delta\boldsymbol{\varepsilon}^{e}$ are the changes in stress and elastic strain at the end of current time increment, respectively. Since the UMAT requires the increment in stress and elastic strain, the constitutive equations are presented here in incremental form.

The total strain within the model is the sum of seven different strain components:

$$\Delta\boldsymbol{\varepsilon}^{total} = \Delta\boldsymbol{\varepsilon}^{e} + \Delta\boldsymbol{\varepsilon}^{pc} + \Delta\boldsymbol{\varepsilon}^{sc} + \Delta\boldsymbol{\varepsilon}^{dc} + \Delta\boldsymbol{\varepsilon}^{th} + \Delta\boldsymbol{\varepsilon}^{ith} + \Delta\boldsymbol{\varepsilon}^{idc}, \tag{11}$$

where $\Delta\boldsymbol{\varepsilon}^{e}$ is the elastic strain, $\Delta\boldsymbol{\varepsilon}^{pc}$ is the primary creep strain, $\Delta\boldsymbol{\varepsilon}^{sc}$ is the secondary creep strain, $\Delta\boldsymbol{\varepsilon}^{dc}$ is the dimensional change strain induced by irradiation, $\Delta\boldsymbol{\varepsilon}^{th}$ is the thermal strain, $\Delta\boldsymbol{\varepsilon}^{ith}$ and $\Delta\boldsymbol{\varepsilon}^{idc}$ are the interaction thermal and dimensional change strains due to creep, respectively. All of these strains are described in more detail below.

4.1. Elastic strain

The elastic strain is related to the stress by means of Hooke's law of linear elasticity, i.e.

$$\boldsymbol{\sigma} = \mathbf{D}\boldsymbol{\varepsilon}^{e}, \tag{12}$$

where the material matrix $\mathbf{D}$ is a function of irradiation temperature and irradiation fluence. The incremental equation for Hooke's law can be written as

$$\Delta\boldsymbol{\sigma} = \widetilde{\mathbf{D}} \cdot \Delta\boldsymbol{\varepsilon}^{e} + \Delta\mathbf{D} \cdot \tilde{\boldsymbol{\varepsilon}}^{e}, \tag{13}$$

where tilde ($\sim$) represents the mean value in current increment. It is assumed that there are no body forces and the stress satisfies the equation of equilibrium, i.e.

$$\sigma_{ij,j} = 0 \tag{14}$$

and the strain–displacement relationships is

$$\varepsilon^{e}_{ij} = \frac{1}{2}(u_{i,j} + u_{j,i}), \tag{15}$$

where the tensor notation has been used and the comma represents partial differentiation.

4.2. Creep strain

In the UK, total irradiation creep strain has traditionally been separated into two creep strain components [3]:

$$\boldsymbol{\varepsilon}^{\text{creep}} = \boldsymbol{\varepsilon}^{\text{pc}} + \boldsymbol{\varepsilon}^{\text{sc}}, \tag{16}$$

where $\boldsymbol{\varepsilon}^{\text{pc}}$ and $\boldsymbol{\varepsilon}^{\text{sc}}$ are the primary and the secondary creep strains, respectively. The primary creep strain, which is also called transient creep, is a recoverable strain and is defined as

$$\boldsymbol{\varepsilon}^{\text{pc}} = 4\varphi \mathrm{e}^{-4\gamma} \int_0^{\gamma} \mathbf{D}_{\text{c}} \boldsymbol{\sigma} \mathrm{e}^{4\gamma'} \,\mathrm{d}\gamma', \tag{17}$$

where $\varphi(T)$ is a parameter dependent on temperature T, γ is the irradiation fluence and $\mathbf{D}_{\text{c}}$ is the usual creep material matrix in which the creep modulus E_{c} is defined as a function of unirradiated modulus, structure term and weight loss as

$$E_{\text{c}} = E_0 \times f_{\text{i}} \times S(\gamma, T) \times W(x)$$

and Poisson's ratio for creep is taken as being the same as the elastic Poisson's ratio and to be invariant to fast neutron irradiation and radiolytic oxidation.

The primary creep is characterised by a rapid deformation which soon decreases in rate with increasing irradiation fluence. To put Eq. (17) in incremental form, first Eq. (17) is rewritten as a differential equation

$$\frac{\mathrm{d}\boldsymbol{\varepsilon}^{\text{pc}}}{\mathrm{d}\gamma} = 4\varphi(\mathbf{D}_{\text{c}}\boldsymbol{\sigma} - \boldsymbol{\varepsilon}^{\text{pc}}) \tag{18}$$

and hence the incremental equation for primary creep can be written as

$$\Delta\boldsymbol{\varepsilon}^{\text{pc}} = 4\varphi(\widetilde{\mathbf{D}}_{\text{c}}\tilde{\boldsymbol{\sigma}} - \tilde{\boldsymbol{\varepsilon}}^{\text{pc}})\,\Delta\gamma. \tag{19}$$

The secondary creep strain, which also called steady state creep, is an irreversible strain and is defined as

$$\boldsymbol{\varepsilon}^{\text{sc}} = \xi(T) \int_0^{\gamma} \mathbf{D}_{\text{c}}\boldsymbol{\sigma}\,\mathrm{d}\gamma', \tag{20}$$

where $\xi(T)$ is a temperature dependent parameter. The secondary creep is characterised by a linear dependence of the creep strain. The incremental equation for secondary creep can be written as

$$\Delta\boldsymbol{\varepsilon}^{\text{sc}} = \xi\widetilde{\mathbf{D}}_{\text{c}}\tilde{\boldsymbol{\sigma}}\Delta\gamma. \tag{21}$$

It is assumed that both parameters φ and ξ are independent of temperature in this paper.

4.3. Thermal strain

The thermal strain is defined as

$$\boldsymbol{\varepsilon}^{\text{th}} = \bar{\boldsymbol{\alpha}}_{(T_{\text{ref}}-T)}(T - T_{\text{ref}}), \tag{22}$$

where $\bar{\boldsymbol{\alpha}}_{(T_{\text{ref}}-T)}$ is the mean coefficient of thermal expansion between temperature T_{ref}–T °C, and T_{ref} is a reference temperature. Differentiating the above equation, we have

$$\delta\boldsymbol{\varepsilon}^{\text{th}} = \delta\bar{\boldsymbol{\alpha}}_{(T_{\text{ref}}-T)}(T - T_{\text{ref}}) + \bar{\boldsymbol{\alpha}}_{(T_{\text{ref}}-T)}\,\delta T. \tag{23}$$

Using Eq. (9), Eq. (23) can be simplified to the following difference equation:

$$\delta\boldsymbol{\varepsilon}^{\text{th}} = \delta\bar{\boldsymbol{\alpha}}_{(20\text{–}120)}(T - T_{\text{ref}}) + \boldsymbol{\alpha}_{\text{i}}\,\delta T \tag{24}$$

and hence the incremental equation for thermal strain can be written as

$$\Delta\boldsymbol{\varepsilon}^{\text{th}} \approx \Delta\bar{\boldsymbol{\alpha}}_{(20\text{–}120)}(T - T_{\text{ref}}) + \boldsymbol{\alpha}_{\text{i}}\,\Delta T. \tag{25}$$

The small orthotropic CTE in semi-isotropic graphite is also accounted for in the code, i.e.

$$\bar{\boldsymbol{\alpha}}_{(T_1-T_2)} = \begin{pmatrix} \bar{\alpha}^1_{(T_1-T_2)} \\ \bar{\alpha}^2_{(T_1-T_2)} \\ \bar{\alpha}^3_{(T_1-T_2)} \end{pmatrix}, \quad \boldsymbol{\alpha}_{\text{i}} = \begin{pmatrix} \alpha^1_{\text{i}} \\ \alpha^2_{\text{i}} \\ \alpha^3_{\text{i}} \end{pmatrix}, \tag{26}$$

where $\bar{\alpha}^1_{(T_1-T_2)}$, $\bar{\alpha}^2_{(T_1-T_2)}$ and $\bar{\alpha}^3_{(T_1-T_2)}$ are mean CTE along orthogonal axis 1, 2 and 3, respectively and similar for instantaneous CTE α_{i}. The mean CTE is a function of fluence, irradiation temperature and actual temperature. The mean CTE over any desired temperature range can be found from Eq. (9). Once the values of CTE in different directions are known, the incremental thermal strain can be calculated from Eq. (25).

4.4. Dimensional change strain

The amount of dimensional change is assumed to be a function of irradiation temperature fluence, temperature and weight loss, and is assumed to be the same in all directions. It is assumed that for a given temperature, the dimensional change against fluence can be represented by

$$\frac{\mathrm{d}\varepsilon^{\text{dc}}}{\mathrm{d}\gamma} = \phi\frac{\mathrm{d}\varepsilon^{\text{dc}}_{\text{A}}}{\mathrm{d}\gamma} + (1-\phi)\frac{\mathrm{d}\varepsilon^{\text{dc}}_{\text{B}}}{\mathrm{d}\gamma}, \tag{27}$$

where $\varepsilon^{\text{dc}}_{\text{A}}$ is the dimensional change strain with maximum effect of weight loss, $\varepsilon^{\text{dc}}_{\text{B}}$ is the dimensional change strain without weight loss effect and ϕ is the fractional parameter between the maximum weight

loss, Curve A, and no weight loss, Curve B. Both terms $\varepsilon_{\mathrm{A}}^{\mathrm{dc}}$ and $\varepsilon_{\mathrm{B}}^{\mathrm{dc}}$ have been determined, therefore the terms $\frac{\mathrm{d}\varepsilon_{\mathrm{A}}^{\mathrm{dc}}}{\mathrm{d}\gamma}$ and $\frac{\mathrm{d}\varepsilon_{\mathrm{B}}^{\mathrm{dc}}}{\mathrm{d}\gamma}$ can be numerically calculated. The incremental form of Eq. (27) can be written as

$$\Delta\varepsilon^{\mathrm{dc}} \approx \left[\phi\frac{\mathrm{d}\varepsilon_{\mathrm{A}}^{\mathrm{dc}}}{\mathrm{d}\gamma} + (1-\phi)\frac{\mathrm{d}\varepsilon_{\mathrm{B}}^{\mathrm{dc}}}{\mathrm{d}\gamma}\right]\Delta\gamma. \tag{28}$$

Hence the change in dimensional change strain can be calculated.

4.5. Interaction strains

The two interaction strains in Eq. (11) are assumed to be a function of irradiation creep in graphite. These are the interaction thermal strain and the interaction dimensional strain.

For small creep strain, the correction in irradiated mean CTE $\hat{\boldsymbol{\alpha}}_{(20\text{–}120)}$ can be calculated using following linear relationship:

$$\hat{\boldsymbol{\alpha}}_{(20\text{–}120)} = \kappa\boldsymbol{\varepsilon}^{\mathrm{ec}}, \tag{29}$$

where

$$\boldsymbol{\varepsilon}^{\mathrm{ec}} = \begin{bmatrix} 1 & -\mu & -\mu & 0 & 0 & 0 \\ -\mu & 1 & -\mu & 0 & 0 & 0 \\ -\mu & -\mu & 1 & 0 & 0 & 0 \\ 0 & 0 & 0 & 1+\mu & 0 & 0 \\ 0 & 0 & 0 & 0 & 1+\mu & 0 \\ 0 & 0 & 0 & 0 & 0 & 1+\mu \end{bmatrix} \begin{pmatrix} \varepsilon_1^{\mathrm{creep}} \\ \varepsilon_2^{\mathrm{creep}} \\ \varepsilon_3^{\mathrm{creep}} \\ \varepsilon_{12}^{\mathrm{creep}} \\ \varepsilon_{13}^{\mathrm{creep}} \\ \varepsilon_{23}^{\mathrm{creep}} \end{pmatrix} \tag{30}$$

is called the effective creep strain, κ is the slope at the origin of the CTE/creep curve and $\mu = 0.5$ is the lateral coefficient. Once the correction in CTE $\hat{\boldsymbol{\alpha}}_{(20\text{–}120)}$ is found, the incremental interaction thermal strain is defined as

$$\Delta\boldsymbol{\varepsilon}^{\mathrm{ith}} \approx \Delta\hat{\boldsymbol{\alpha}}_{(20\text{–}120)}(T - T_{\mathrm{ref}}) + \hat{\boldsymbol{\alpha}}_{(20\text{–}120)}\Delta T. \tag{31}$$

Since the interaction thermal strain is a correction in CTE due to the total creep strain. The expression in Eq. (31) is same as the definition of the thermal strain given in Eq. (25).

We have seen how the total creep strain modifies the CTE. However, the dimensional change strain appears to be a function of CTE, therefore creep strain may be expected to modify the dimensional change. Kelly and Burchell [19] proposed an interaction dimensional change strain is defined as

$$\boldsymbol{\varepsilon}^{\mathrm{idc}} = \int_0^{\gamma}\left(\frac{\hat{\boldsymbol{\alpha}}_{(20\text{–}120)}}{(\alpha_c - \alpha_a)}\right)\frac{\mathrm{d}X_T}{\mathrm{d}\gamma}\mathrm{d}\gamma', \tag{32}$$

where α_c and α_a are the crystallite CTE in 'a' and 'c' directions, respectively. The function X_T is the so-called shape factor for the graphite crystallite which is given by the difference in the crystallite dimensional change in the 'a' and 'c' directions defined as

$$X_T = \frac{\Delta X_{\mathrm{c}}}{X_{\mathrm{c}}} - \frac{\Delta X_a}{X_a}, \tag{33}$$

where X_T is a function of irradiation temperature and fast neutron fluence and has been obtained from irradiation experiments on highly orientated pyrolytic graphite (HPOG). Hence the crystal shape term $\mathrm{d}X_T/\mathrm{d}\gamma$ can been found and the incremental equation for Eq. (32) can be calculated using

$$\Delta\boldsymbol{\varepsilon}^{\mathrm{idc}} \approx \left(\frac{\widehat{\boldsymbol{\alpha}}_{(20\text{–}120)}}{\alpha_c - \alpha_a}\right)\frac{\mathrm{d}X_T}{\mathrm{d}\gamma}\Delta\gamma, \tag{34}$$

where $\widehat{\boldsymbol{\alpha}}_{(20\text{–}120)}$ is the average value of corrected CTE at current increment.

The CTE correction term $\hat{\boldsymbol{\alpha}}_{(20\text{–}120)}$ is a function of the total creep strain. Since both the interaction strains are functions of the CTE correction term, both interaction strains are implicit functions of the total creep strain.

5. Numerical technique

In this section, the implementation of the program is described. The material model has been implemented into ABAQUS [7] via user material subroutine (UMAT). If interaction strains are not included in an analysis, all the strain can be calculated explicitly. From the previous section it can be noticed that both interaction strains are implicit functions of the total creep strain. Hence a predictor–corrector approach has been developed to evaluate the interaction strains.

At a current time step i, the thermal and dimensional change strains are determined first. It is assumed that the average value in an increment can be approximately calculated by the central difference method, i.e.

$$\begin{aligned} \tilde{\boldsymbol{\sigma}} &= \boldsymbol{\sigma}_{\mathrm{i}} + \frac{\Delta\boldsymbol{\sigma}}{2}, \\ \tilde{\boldsymbol{\varepsilon}} &= \boldsymbol{\varepsilon}_{\mathrm{i}} + \frac{\Delta\boldsymbol{\varepsilon}}{2}. \end{aligned} \tag{35}$$

In the predictor step, all the strains except the interaction strains are considered. Using Eqs. (13) and (35), the primary creep (19) and the secondary creep (21) strains can be written as

$$\Delta\boldsymbol{\varepsilon}^{\mathrm{pc}} - \frac{\varphi\,\Delta\gamma(2\phi_1+\phi_2)}{1+2\varphi\,\Delta\gamma}\Delta\boldsymbol{\varepsilon}^{\mathrm{e}} = \frac{2\varphi\,\Delta\gamma\phi_2\boldsymbol{\varepsilon}_{\mathrm{i}}^{\mathrm{e}} + 4\varphi\,\Delta\gamma(\widetilde{\mathbf{D}}_{\mathrm{c}}\boldsymbol{\sigma}_{\mathrm{i}} - \boldsymbol{\varepsilon}_{\mathrm{i}}^{\mathrm{pc}})}{1+2\varphi\,\Delta\gamma}, \tag{36}$$

$$\Delta\boldsymbol{\varepsilon}^{\mathrm{sc}} - \xi\,\Delta\gamma\left(\frac{2\phi_1+\phi_2}{4}\right)\Delta\boldsymbol{\varepsilon}^{\mathrm{e}} = \xi\,\Delta\gamma\left(\widetilde{\mathbf{D}}_{\mathrm{c}}\boldsymbol{\sigma}_{\mathrm{i}} + \frac{\phi_2\boldsymbol{\varepsilon}_{\mathrm{i}}^{\mathrm{e}}}{2}\right), \tag{37}$$

where $\phi_1 = E/E_{\mathrm{c}}$ is the ratio of Young's modulus to creep modulus and $\phi_2 = \Delta E/E_{\mathrm{c}}$ is the ratio of change in Young's modulus to creep modulus. The total strain in Eq. (11) can be written as

$$\Delta\boldsymbol{\varepsilon}^{\mathrm{e}} + \Delta\boldsymbol{\varepsilon}^{\mathrm{pc}} + \Delta\boldsymbol{\varepsilon}^{\mathrm{sc}} = \Delta\boldsymbol{\varepsilon}^{\mathrm{total}} - \Delta\boldsymbol{\varepsilon}^{\mathrm{dc}} - \Delta\boldsymbol{\varepsilon}^{\mathrm{th}}. \tag{38}$$

Now we have three Eqs. (36)–(38) with known right-hand sides and three unknowns $\Delta\boldsymbol{\varepsilon}^{\mathrm{e}}$, $\Delta\boldsymbol{\varepsilon}^{\mathrm{pc}}$ and $\Delta\boldsymbol{\varepsilon}^{\mathrm{sc}}$, which can be solved easily using linear algebra. The solution for $\Delta\boldsymbol{\varepsilon}^{\mathrm{e}}$ is

$$\Delta\boldsymbol{\varepsilon}^{\mathrm{e}} = \frac{\Delta\boldsymbol{\varepsilon}^{\mathrm{total}} - \Delta\boldsymbol{\varepsilon}^{\mathrm{dc}} - \Delta\boldsymbol{\varepsilon}^{\mathrm{th}} - \xi\,\Delta\gamma\widetilde{\mathbf{D}}_{\mathrm{c}}\boldsymbol{\sigma}_{\mathrm{i}} - \frac{4\varphi\,\Delta\gamma(\widetilde{\mathbf{D}}_{\mathrm{c}}\boldsymbol{\sigma}_{\mathrm{i}} - \boldsymbol{\varepsilon}_{\mathrm{i}}^{\mathrm{pc}})}{1+2\varphi\,\Delta\gamma} - \phi_2\,\Delta\gamma\left(\frac{2\varphi}{1+2\varphi\,\Delta\gamma} + \frac{\xi}{2}\right)\boldsymbol{\varepsilon}_{\mathrm{i}}^{\mathrm{e}}}{1 + \Delta\gamma\left(\frac{\varphi}{1+2\varphi\,\Delta\gamma} + \frac{\xi}{4}\right)(2\phi_1+\phi_2)}. \tag{39}$$

Once the solution for $\Delta\boldsymbol{\varepsilon}^{\mathrm{e}}$ is found, the solutions for $\Delta\boldsymbol{\varepsilon}^{\mathrm{pc}}$ and $\Delta\boldsymbol{\varepsilon}^{\mathrm{sc}}$ can be found by substituting $\Delta\boldsymbol{\varepsilon}^{\mathrm{e}}$ into Eqs. (36) and (37).

Once we have the solutions for $\Delta\boldsymbol{\varepsilon}^{\mathrm{pc}}$ and $\Delta\boldsymbol{\varepsilon}^{\mathrm{sc}}$, accordingly the total creep strain can be found and hence both interaction strains. In the corrector step, we update Eq. (38) as

$$\Delta\boldsymbol{\varepsilon}^{\mathrm{e}} + \Delta\boldsymbol{\varepsilon}^{\mathrm{pc}} + \Delta\boldsymbol{\varepsilon}^{\mathrm{sc}} = \Delta\boldsymbol{\varepsilon}^{\mathrm{total}} - \Delta\boldsymbol{\varepsilon}^{\mathrm{dc}} - \Delta\boldsymbol{\varepsilon}^{\mathrm{th}} - \Delta\boldsymbol{\varepsilon}^{\mathrm{idc}} - \Delta\boldsymbol{\varepsilon}^{\mathrm{ith}}. \tag{40}$$

A new approximation for $\Delta\boldsymbol{\varepsilon}^{\mathrm{e}}$ can be obtained by replacing Eq. (38) with Eq. (40) in the predictor step, and hence the new approximation can be found for the creep strains and the interaction strains.

In theory, improved approximations to $\Delta\boldsymbol{\varepsilon}^{\mathrm{e}}$ can be obtained by iterating the corrector step. In practice, since $\Delta\boldsymbol{\varepsilon}^{\mathrm{e}}$ converges to the actual approximation given by the implicit formula rather than to the solution of $\Delta\boldsymbol{\varepsilon}^{\mathrm{e}}$, it is more efficient to use a reduction in the step size if improved accuracy is needed.

6. Numerical example

As an example, a simple three-dimensional model has been analysed as depicted in Fig. 4. The model represents one-eighth of a half-height graphite moderator brick used in a hypothetical reactor design. The internal radius r_{i} and external radius r_{e} are 150 mm and 300 mm, respectively. The model height is 250 mm. Fig. 5 shows the dimension of the model cross-section. The radius of the corner at the root of the keyway is 6 mm. Symmetry condition are applied on both radial boundaries and on the top surface.

In order to perform the stress analysis, four field variables are required. They are irradiation fluence, irradiation temperature, weight loss and radiolytic oxidation rate. Simple profiles for these field variables have been created to model the reactor conditions. It is assumed that all field variables vary in radial direction but are uniform along the circumferential direction and the height of the brick. Fig. 6 shows the irradiation fluence profile at the end of 30 full power years (fpy). It is assumed that the maximum and minimum values for these field variables occur at the internal radius and external radius, respectively. Both irradiation fluence and weight loss are assumed to vary linearly with time whereas the temperature and the oxidation rate are assumed to remain constant through the whole reactor life. Before reactor start-up and after shutdown the brick is assumed to be at a uniform ambient temperature. The material properties used in the analysis are taken from Brocklehurst and Kelly [27].

The undeformed shape of the brick is shown in Fig. 7 together with the irradiated brick shape after 30 full power years. The graphite moderator brick changes its shape during its service life and the overall dimensions become smaller; both the height and the bore radius of the brick decrease by about 3%. When fuel bricks are shrinking the hoop stresses are tensile at the bore and compressive at the periphery, leading to keyway closure and keyway dovetailing. After the turnaround as the graphite swells the situation is reversed and the keyways start to open.

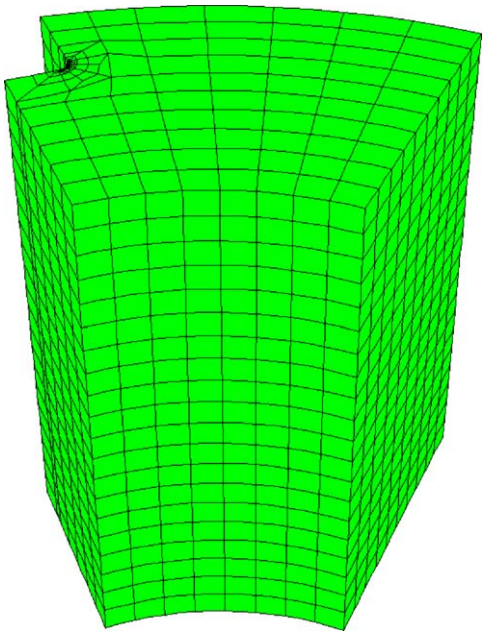

Fig. 4. Finite element mesh profile of a hypothetical graphite moderator brick; the length of the model is 250 mm, symmetry condition is applied on both radial boundaries and on the top surface.

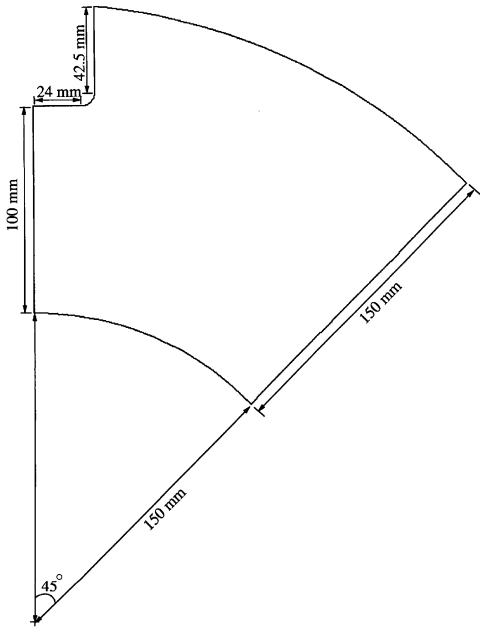

Fig. 5. Dimensions of the graphite brick cross-section.

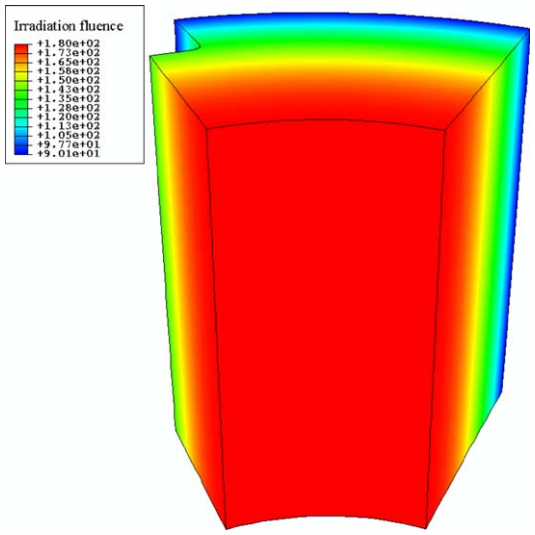

Fig. 6. Irradiation fluence profile at the end of 30 fpy, maximum fluence at the inner radius and minimum fluence at the outer radius.

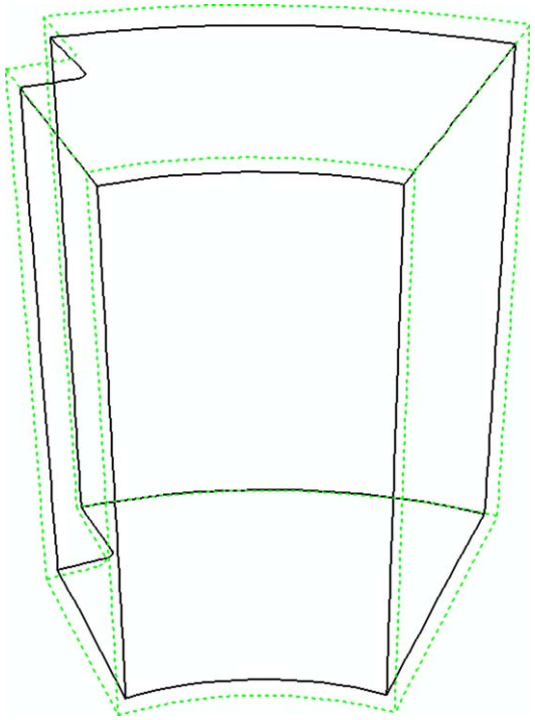

Fig. 7. Comparison of an unirradiated brick (dotted line) with an irradiated brick (solid line) after 30 fpy.

The bore hoop stresses at three height positions are shown in Fig. 8. Initially, at start-up compressive stresses are caused by the radial temperature variation; the temperature being the highest at the bore. These thermal stresses are quickly relieved by the primary creep strain. As the irradiation induced shrinkage of the graphite is initially highest

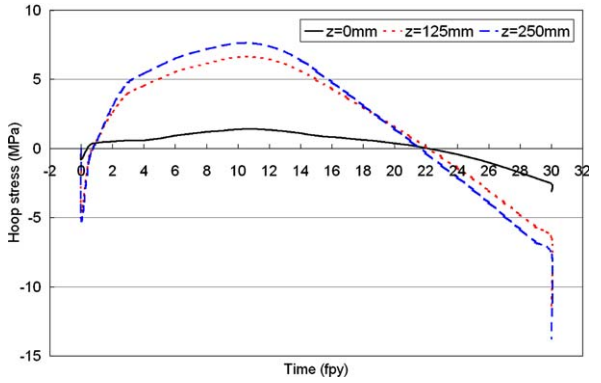

Fig. 8. Time history of the bore hoop stress at three heights.

in the high temperature region near the bore, the stresses quickly change sign with increasing fluence and tensile stresses are developed at the bore. Towards the end of the brick life, compressive stresses develop again at the bore due to expansion of the graphite after turnaround. The crossover in stress occurs around 22 fpy. It is important to note that the shut-down stresses are higher than the operating stresses. This is because the initial thermal stresses are crept out during operation, but return in the opposite sense at shut-down and add to the shrinkage stresses, in addition the irradiation change in CTE also increases the shut-down stresses.

The maximum tensile hoop stresses at $z = 0$ mm, 125 mm and 250 mm are 1.41 MPa, 6.65 MPa and 7.66 MPa, respectively. It is clear that the stresses vary with height along the brick length. The stress level is highest at $z = 250$ mm (i.e. middle of the brick). The stress level is lowest at $z = 0$ mm (i.e. bottom of the brick).

The stress profiles at the keyway are shown in Fig. 9 and are in opposite in sign to those in the bore. The initial keyway stress is tensile at the keyway. As irradiation damage began the stresses change sign and compressive stresses develop. The stresses change sign again due to dimensional change turnaround.

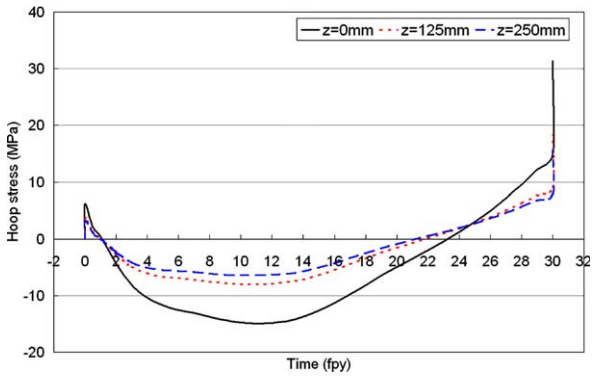

Fig. 9. Time history of the keyway hoop stress at three heights.

The maximum compressive hoop stresses at $z = 0$ mm, 125 mm and 250 mm are 14.95 MPa, 7.98 MPa and 6.43 MPa respectively. Hence, the maximum compressive hoop stress now occurs at the bottom of the brick.

7. Conclusions

There are significant property changes in nuclear graphite components due to fast neutron irradiation and radiolytic oxidation. These changes lead to component deformations and stresses that must be accounted for in graphite component life time assessments. A complex material model for nuclear graphite under irradiation and radiolytic oxidation conditions has been derived. The model is largely empirical and is based on measurements made on graphite samples irradiated in material test reactors. A predictor–corrector procedure has been developed to solve the material model constitutive equations. The model has been implemented in, and can be used together with finite element program ABAQUS to perform irradiated graphite stress analyses. A stress analysis is presented for a three-dimensional hypothetical nuclear graphite brick. The numerical results predict that the maximum tensile stress at the bore occurs at the middle height of the brick, whereas the maximum compressive stress at the keyway occurs at the bottom of the brick.

References

[1] K.H. Dent, in: W. Marshall (Ed.), Nuclear Power Technology, Reactor Technology, vol. 1, Clarendon, Oxford, 1986, p. 138.
[2] R.F. Pocock, Nuclear Power: Its Development in the United Kingdom, The Institution of Nuclear Engineers, England, 1977.
[3] B.T. Kelly, J.E. Brocklehurst, J. Nucl. Mater. 65 (1977) 79.
[4] Y.T. Chang, Y.R. Rashid, Nucl. Eng. Des. 14 (1970) 181.
[5] T. Iyoku, M. Ishihara, H. Shirai, J. Nucl. Sci. Technol. 28 (1991) 921.
[6] P.G. Harper, User Guide to BERSAFE Phase III for Reactor Graphite, RD/B/N4797, 1980.
[7] ABAQUS, Hibbit, Karlsonn and Sorensen, 2005.
[8] H.J. Whittaker, Influence of creep Poisson's ratio on irradiation induced self stress in graphite, in: 4th UK ABAQUS User Group Conference, 1988.
[9] H. Li, B.J. Marsden, S.L. Fok, Nucl. Eng. Des. 232 (2004) 237.

[10] S. Mrozowski, Mechanical strength, thermal expansion and structure of cokes and carbons, in: Proceedings of the 1st Conference on Carbon, 1956, p. 31.
[11] T. Oku, M. Eto, Nucl. Eng. Des. 143 (1993) 239.
[12] M.W. Thompson, S.B. Wright, J. Nucl. Mater. 16 (1965) 146.
[13] J.H.W. Simmons, Radiation Damage in Graphite, Pergamon, 1965.
[14] W.N. Reynolds, P.A. Thrower, Philos. Mag. 12 (1965) 573.
[15] J.V. Best, W.J. Stephen, A.J. Wickham, Prog. Nucl. Energy 16 (1985) 127.
[16] B.T. Kelly, Prog. Nucl. Energy 16 (1985) 73.
[17] J.E. Brocklehurst, in: P.L. Walker, P.A. Thrower (Eds.), Chemistry and Physics of Carbon, vol. 13, 1977, p. 145.
[18] D.K.L. Tsang, B.J. Marsden, Modelling of nuclear graphite behaviour under irradiation conditions, in: Proceeding of Ageing Management of Graphite Reactor Cores, Cardiff, 2005.
[19] B.T. Kelly, T.D. Burchell, Carbon 32 (1994) 119.
[20] T. Oku, K. Fujisaki, M. Eto, J. Nucl. Mater. 152 (1988) 225.
[21] D.K.L. Tsang, B.J. Marsden, S.L. Fok, G. Hall, Carbon 43 (2005) 2902.
[22] B.T. Kelly, Carbon 30 (1992) 379.
[23] J.E. Brocklehurst, B.T. Kelly, Carbon 31 (1993) 179.
[24] G.B. Neighbour, J. Phys. D: Appl. Phys. 33 (2000) 2966.
[25] B.T. Kelly, Carbon 20 (1982) 3.
[26] B.T. Kelly, T.D. Burchell, Carbon 32 (1994) 499.
[27] J.E. Brocklehurst, B.T. Kelly, Carbon 31 (1993) 155.